Supporting information

Microwave-Assisted One-Pot Sol-Gel Synthesis of Tungsten Silicate Microspheres with Dispersed WO_x and Their Activity in Ethanol Dehydration

David Skoda [1*], Tomas Pokorny [2], Barbora Hanulikova [1], Ales Styskalik [2*], Zuzana Hlavenkova [3], Lucie Simonikova [2], Jan Varada [2], Lucie Leonova [2], Ivo Kuritka [1], Claude Poleunis [4], Damien P. Debecker [4*]

[1] Centre of Polymer Systems, Tomas Bata University in Zlín, tr. Tomase Bati 5678, Zlín, CZ-76001, Czech Republic
[2] Department of Chemistry, Faculty of Science, Masaryk University, Kotlarska 2, Brno, CZ-61137, Czech Republic
[3] Central European Institute of Technology, Masaryk University, Kamenice 5, Brno, CZ 62500, Czech Republic
[4] Institute of Condensed Matter and Nanosciences (IMCN), Université catholique de Louvain (UCLouvain), Place Louis Pasteur 1, 1348 Louvain-La-Neuve, Belgium

* dskoda@utb.cz

* styskalik@chemi.muni.cz

* damien.debecker@uclouvain.be

Table of contents

1 Hybrid tungsten silicate solid precursors

Table 1S. Precursor amounts and hybrid materials yields.

sample	$W(CO)_6$		H_2NDC		APTES		yield[a]
	m [mg]	n [mmol]	m [mg]	n [mmol]	m [g]	n [mmol]	[mg]
12W-SiO_2	174.8	0.50	233.8	1.08	1.1863	5.36	678
6W-SiO_2	84.2	0.24	233.3	1.08	1.1814	5.34	645
2W-SiO_2	24.2	0.07	233.7	1.08	1.1858	5.36	605

[a] yield of as-prepared dried product (hybrid tungsten silicate microspheres)

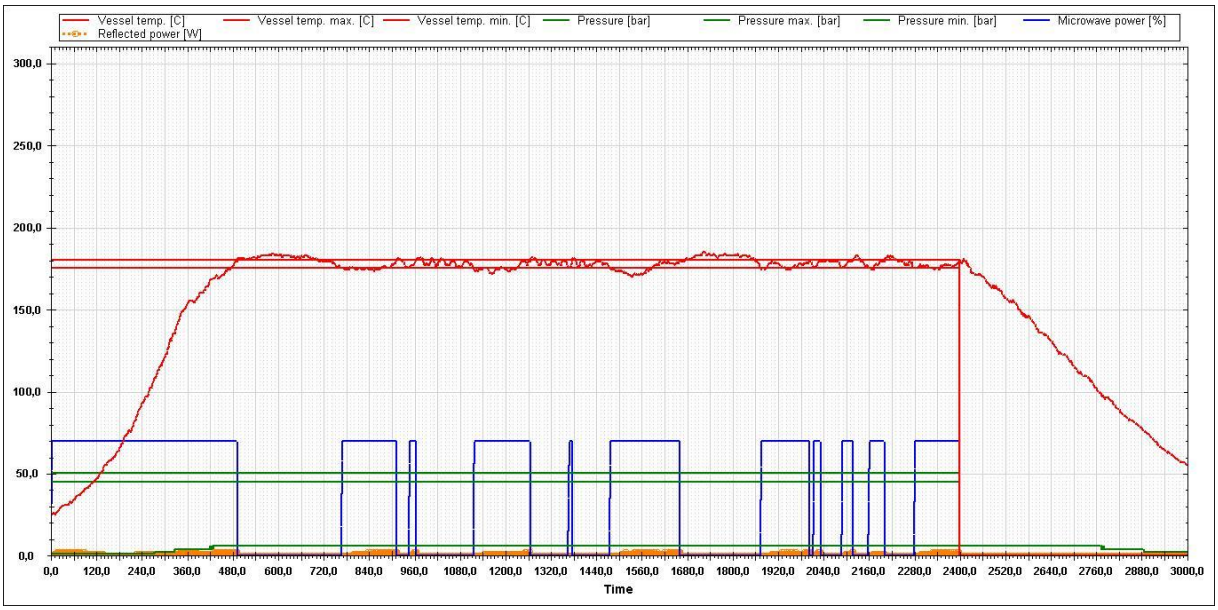

Figure 1S. MW-reactor record of 12W-NDC precursor solution preparation.

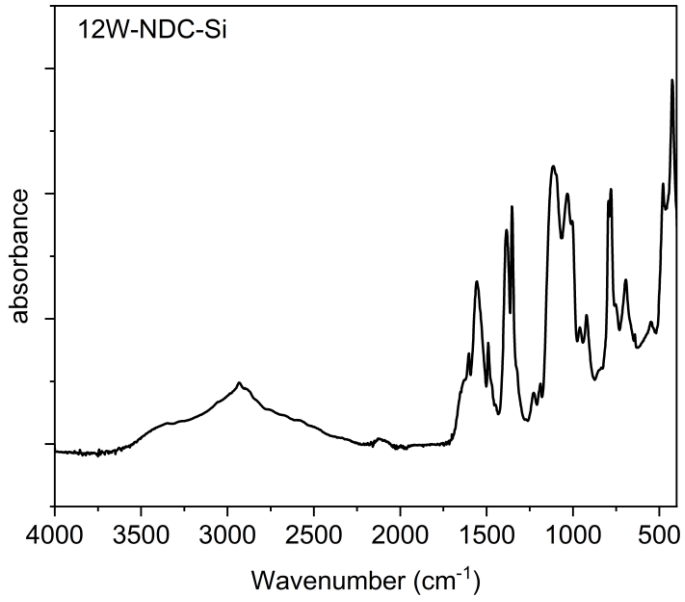

Figure 2S. FTIR spectrum of 12W-NDC-Si sample.

FTIR spectra of all W-NDC-Si solid precursor (Figure 2S) exhibited an intense absorption bands at 1353 and 1386 cm^{-1} which is attributed to the symmetric stretching modes of carboxylate groups in NDC linker[1,2] while the band at 780 cm^{-1} is characteristic for C-H vibrations in aromatic rings. The vibrational bands located in regions 1494 and 1560 cm^{-1} are ascribed to the asymmetric stretching modes of carboxylate groups. The Si–O–Si linkages are characterized by vibrational bands located at 1116, 1034, and 1007 cm^{-1}.[3,4] A vibrational band with wavenumber 962 cm^{-1} is indicative for Si–OH/Si–O–W species.[4] Further, the vibrational band of W=O bonds is found at 921 cm^{-1}.[4]

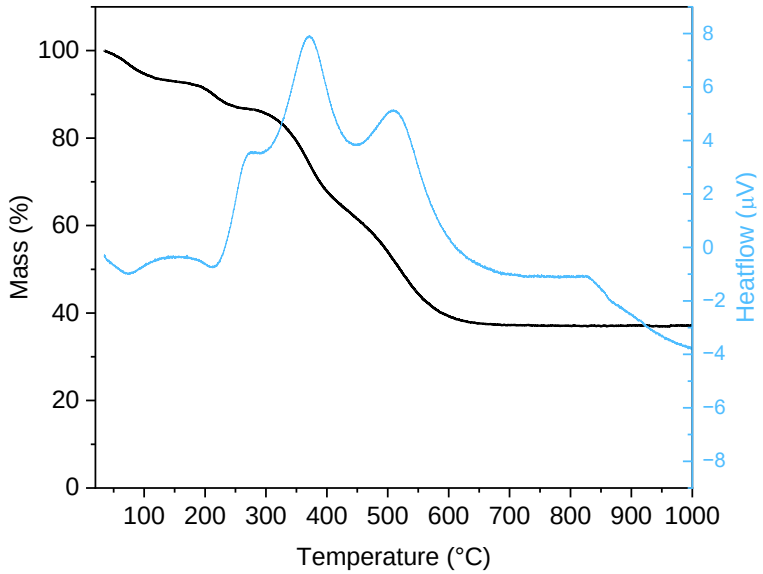

Figure 3S. TG/DSC analysis of 12W-NDC-Si sample

A residual mass of 37.1% was obtained after TG analysis in air at 1000 °C (Figure 3S). Several mass-loss steps are evident on the TG curve. The first loss, occurring between 30 and 175 °C (7.5%), corresponds to the release of residual DMF solvent. The second loss (15.4%) between 175 and 360 °C is attributed to the decomposition of the 3-aminopropyl groups originating from APTES.[5] In contrast, the final mass loss (39.0%) in the range of 350–610 °C is associated with oxidation and decomposition of the NDC linker. The TG data are presented together with a heat-flow curve, which shows three exothermic events corresponding to the oxidation of both the 3-aminopropyl groups and the NDC linker.

2 Tungsten silicate microspheres

2.1 SEM images

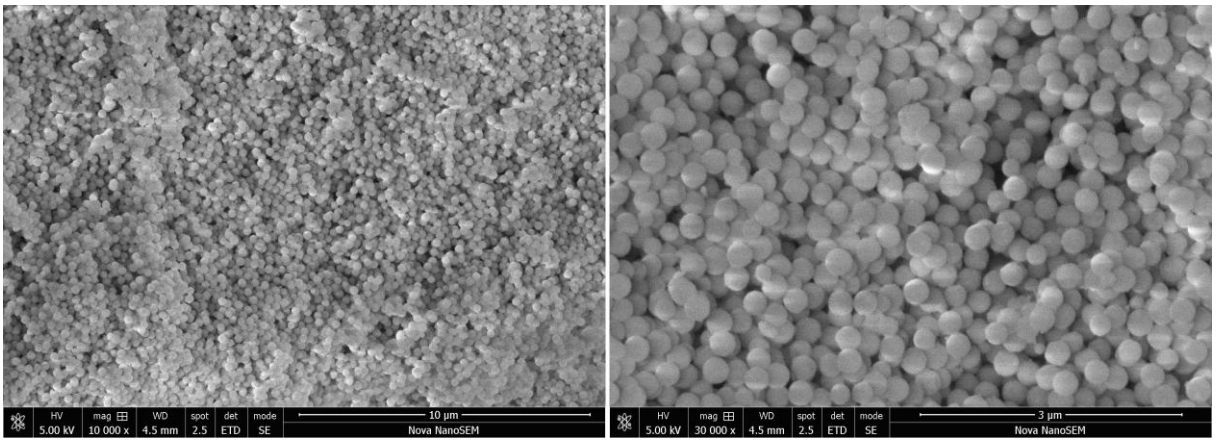

Figure 4S. SEM images of 12W-SiO_2 catalyst sample.

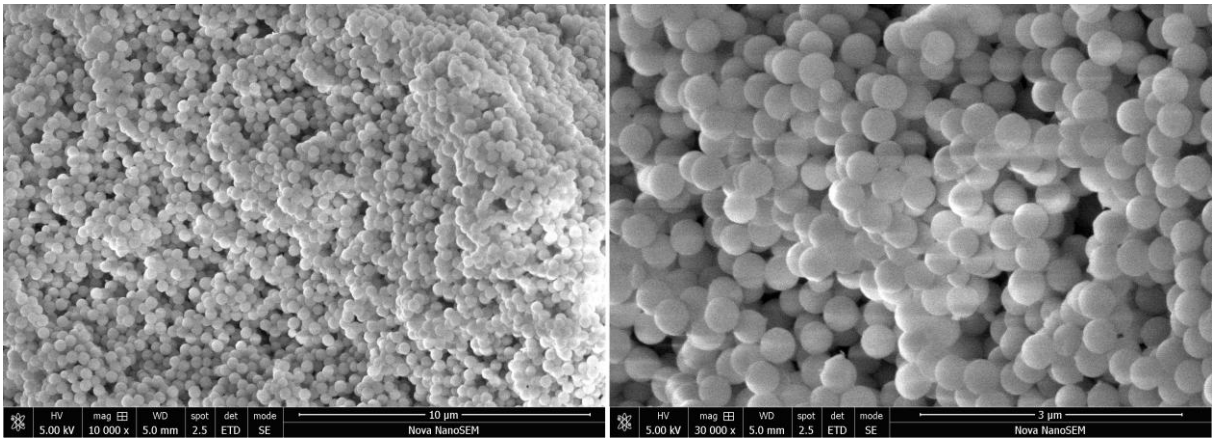

Figure 5S. SEM images of 6W-SiO_2 catalyst sample.

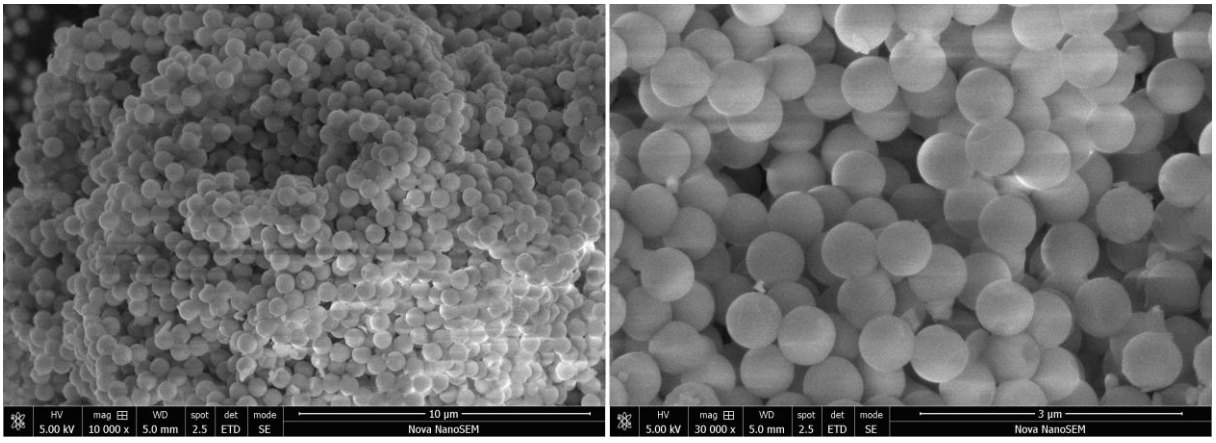

Figure 6S. SEM images of 2W-SiO_2 catalyst sample.

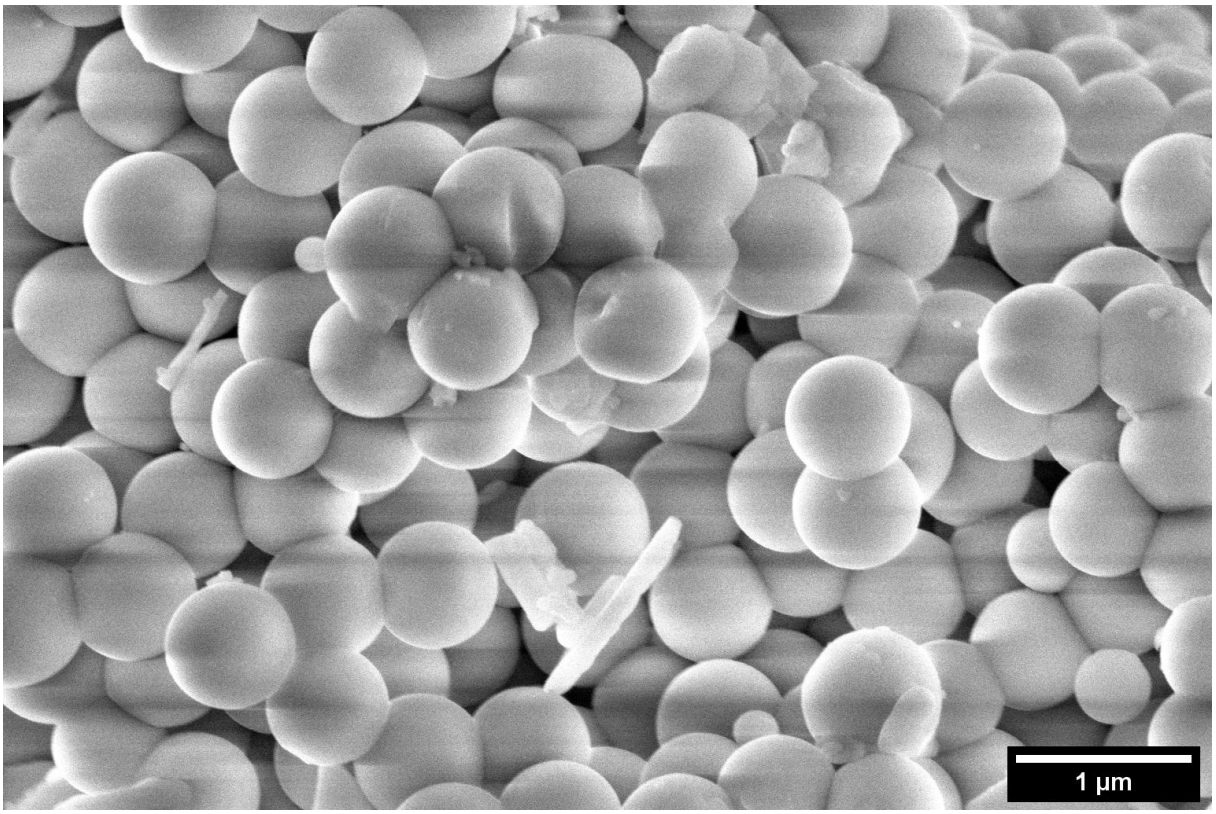

Figure 7S. SEM image of the 4W-SiO_2-imp sample.

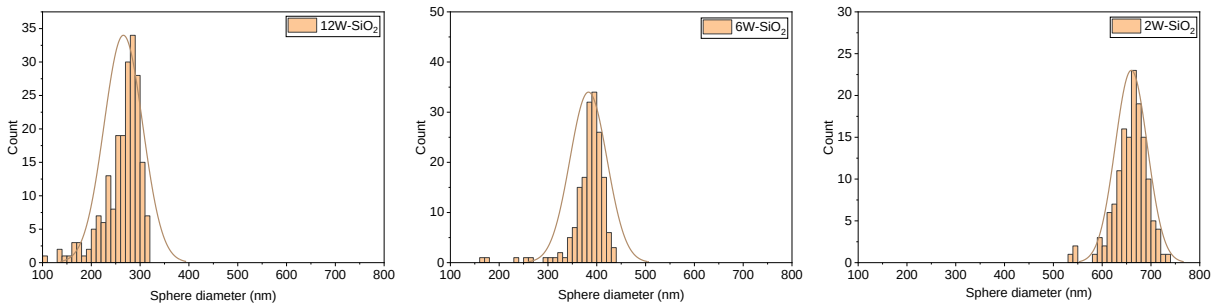

Figure 8S. SEM-derived microsphere diameters of 12W-SiO_2, 6W-SiO_2, and 2W-SiO_2 catalyst samples.

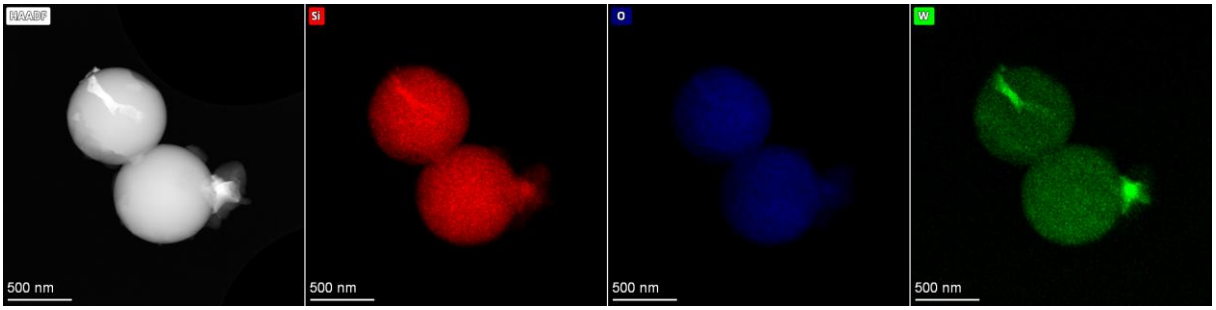

Figure 9S. HAADF and STEM-EDS images of the 4W-SiO_2-imp sample.

2.2 Surface area of 12W-SiO_2-WI

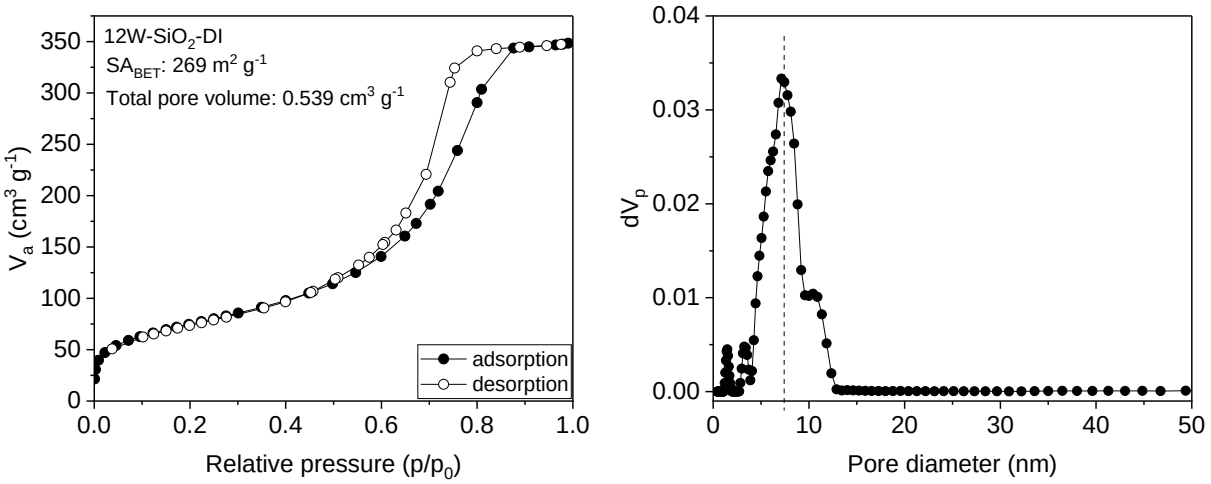

Figure 10S. Nitrogen adsorption/desorption isotherms of 12W-SiO_2-WI sample (left) and its pore size distribution determined by NLDFT method (right).

2.3 XPS spectra of W-SiO_2

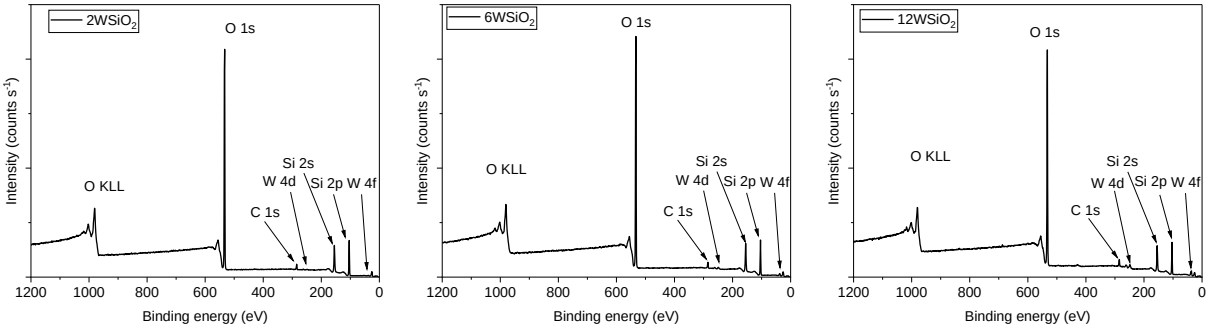

Figure 11S. Survey XPS scans of 2W-SiO_2, 6W-SiO_2, and 12W-SiO_2 catalyst samples.

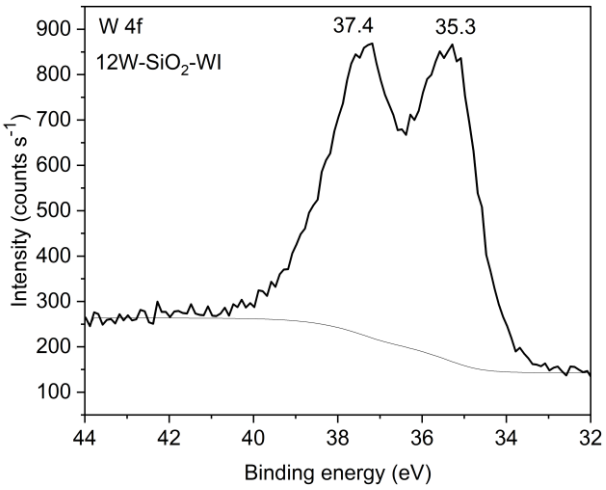

Figure 12S. W 4f spectrum of 12W-SiO_2-WI sample.

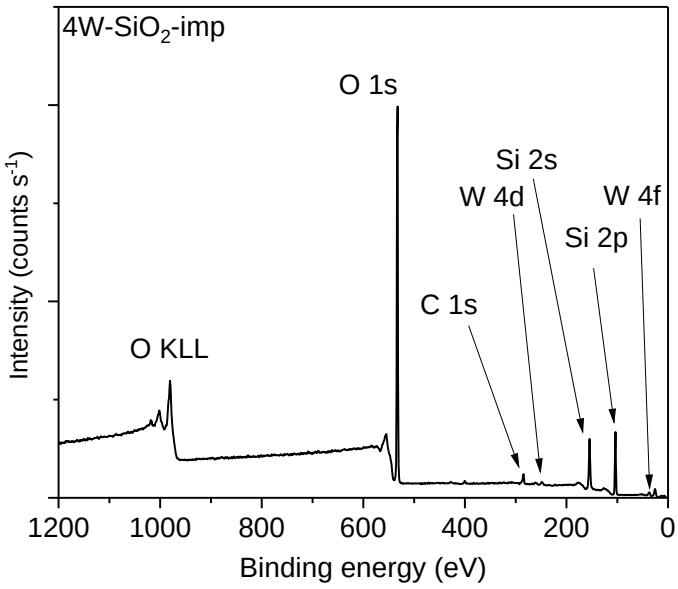

Figure 13S. Survey XPS scan of 4W-SiO_2-imp.

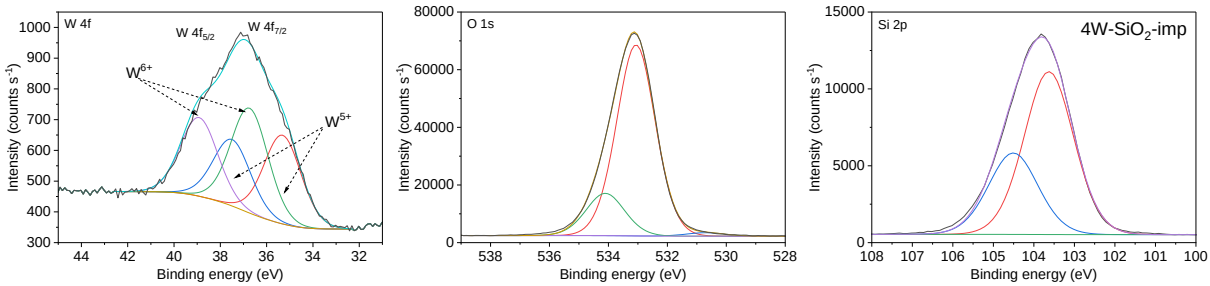

Figure 14S. W 4f, O 1s, and Si 2p XPS spectra of 4W-SiO_2-imp catalyst sample.

Table 2S. Surface compositions of the W-SiO_2 catalysts determined by XPS method

	wt.% XPS			
sample	W	Si	O	C
2W-SiO_2	0.90	52.10	43.17	3.82
6W-SiO_2	2.75	50.16	43.52	3.56
12W-SiO_2	7.87	48.73	40.35	3.05
12W-SiO_2-WI	7.31	52.1	38.90	1.68
4W-SiO_2-imp	2.63	51.60	42.15	3.59

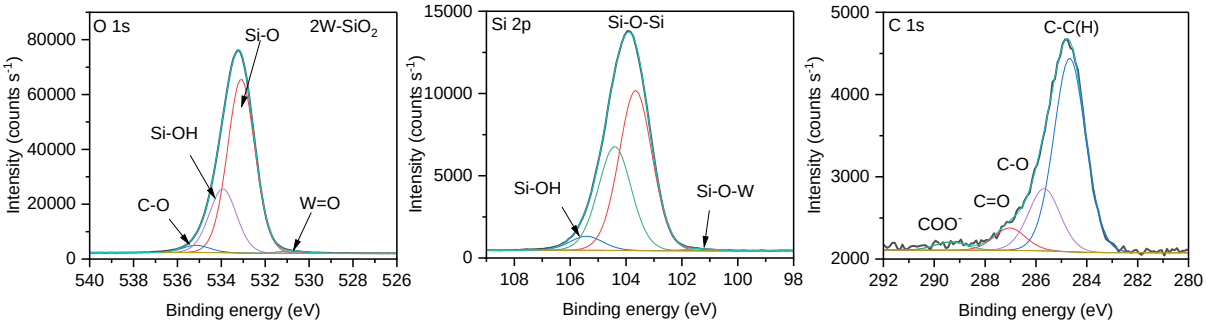

Figure 15S. O 1s, Si 2p, and C 1s XPS spectra of 2W-SiO_2 catalyst sample.

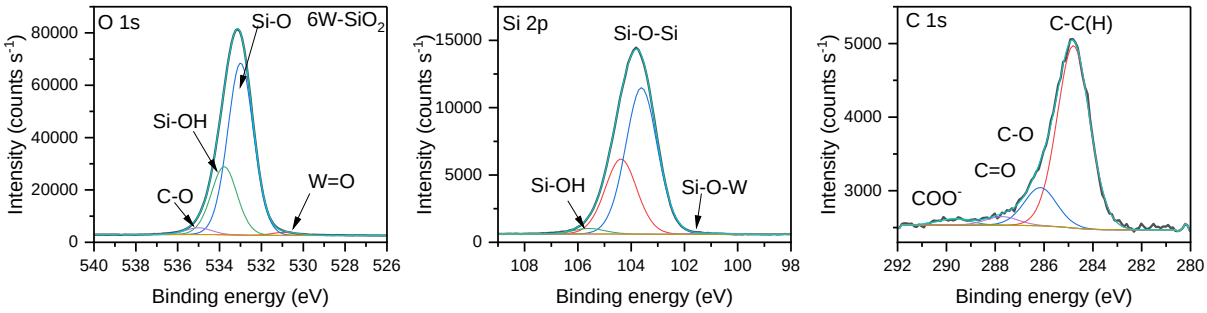

Figure 16S. O 1s, Si 2p, and C 1s XPS spectra of 6W-SiO_2 catalyst sample.

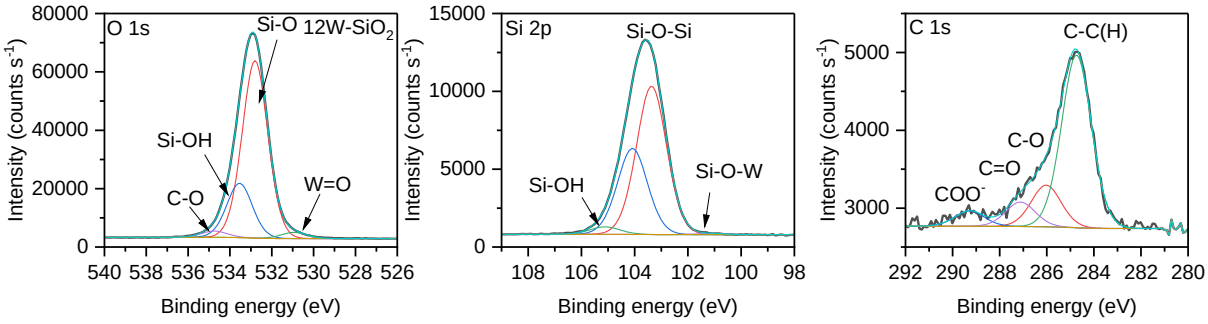

Figure 17S. O 1s, Si 2p, and C 1s XPS spectra of 12W-SiO_2 catalyst sample.

2.4 TOF-SIMS results

Table 3S. List of all W-based clusters identified by ToF-SIMS and considered in the formula reflecting total W content.

cluster	Mass (u)
$^{182}WO_3^-$	229.9326
WO_3^-	231.9355
$^{186}WO_3^-$	233.9397
$^{182}WO_4^-$	245.9271
WO_4^-	247.9321
$^{186}WO_4^-$	249.9322
$^{182}WO_5Si^-$	289.8973
WO_5Si^-	291.9032
$^{186}WO_5Si^-$	293.9038
$^{182}WO_6Si^-$	305.8922
WO_6Si^-	307.8975
$^{186}WO_6Si^-$	309.9019
$^{182}WO_7Si_2^-$	349.8605
$WO_7Si_2^-$	351.8629
$^{186}WO_7Si_2^-$	353.8651
$W_2O_6^-$	463.8679
$W_3O_9^-$	695.807

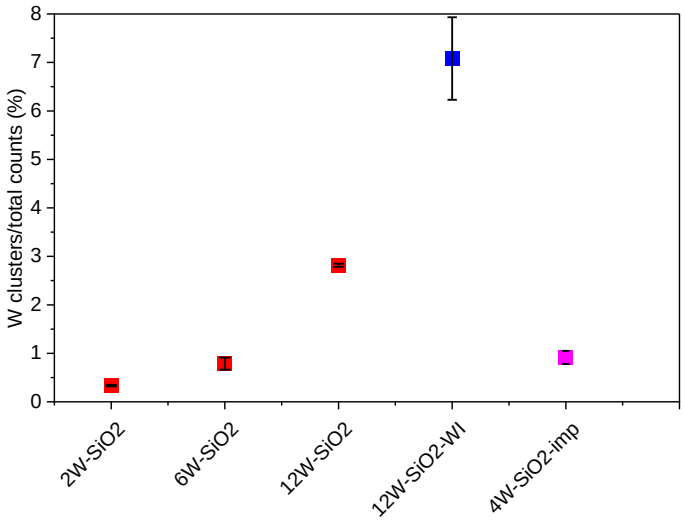

Figure 18S. The total proportion of W-containing clusters from W-SiO_2-based microspheres (i.e., the sum of the intensity for each W-containing anion normalized by the total count). Error bars are standard deviation of each data set (3 analyses per sample).

2.5 Pyridine adsorption

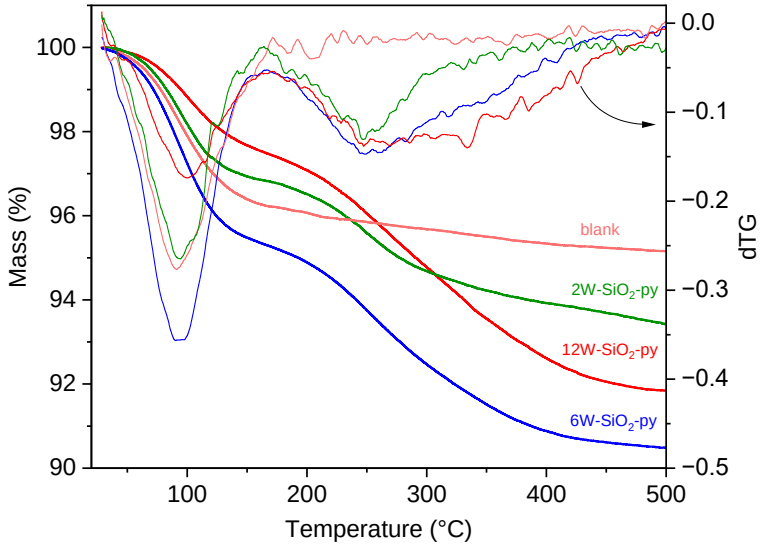

Figure 19S. TG and dTG curves of 12W-SiO_2, 6W-SiO_2, and 2W-SiO_2 catalyst samples after pyridine adsorption. Analysis was performed in the atmosphere of nitrogen.

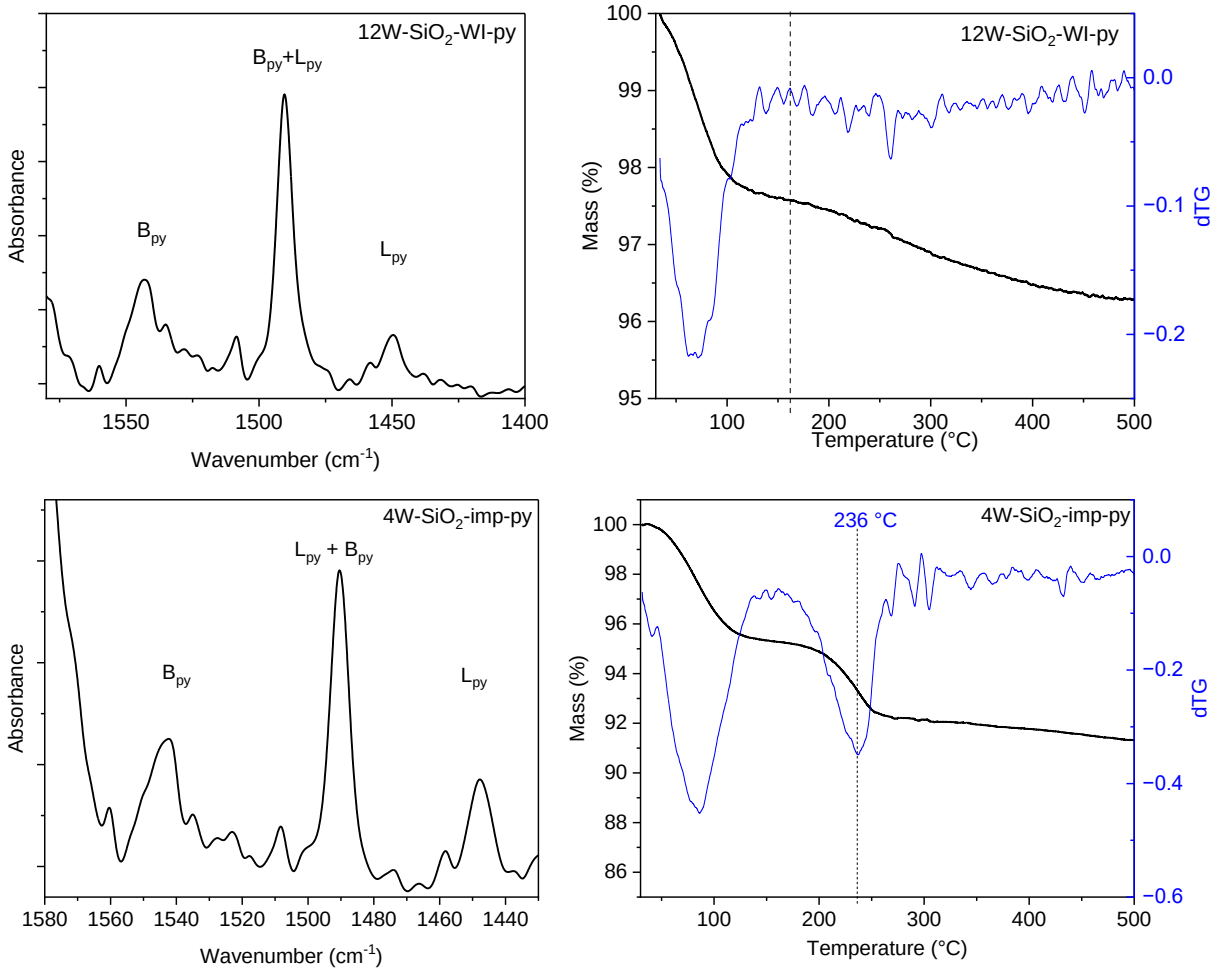

Figure 20S. FTIR spectrum of 12W-SiO_2-WI and 4W-SiO_2-imp catalyst samples after pyridine adsorption (left). TG and dTG curves of 12W-SiO_2-WI and 4W-SiO_2-imp catalyst samples after pyridine adsorption (right). Analysis was performed in the atmosphere of nitrogen.

Table 4S. Mass loss of pyridine adsorbed on impregnation-based samples determined by TGA

sample	pyridine mass loss TG [%]	pyridine [mmol/g]
4W-SiO_2-imp	3.10	0.39
12W-SiO_2-WI-py	1.27	0.16

2.6 Water contact angle

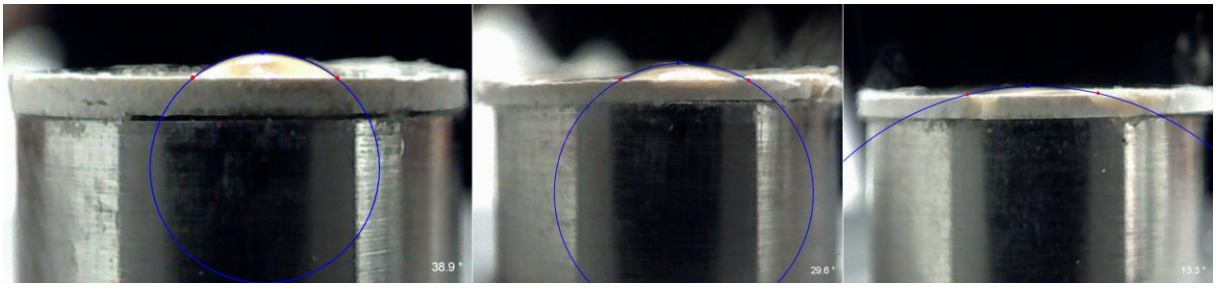

Figure 21S. Water contact angle images. From left to right: 2W-SiO_2, 6W-SiO_2, and 12W-SiO_2.

3 W-SiO_2 catalytic studies

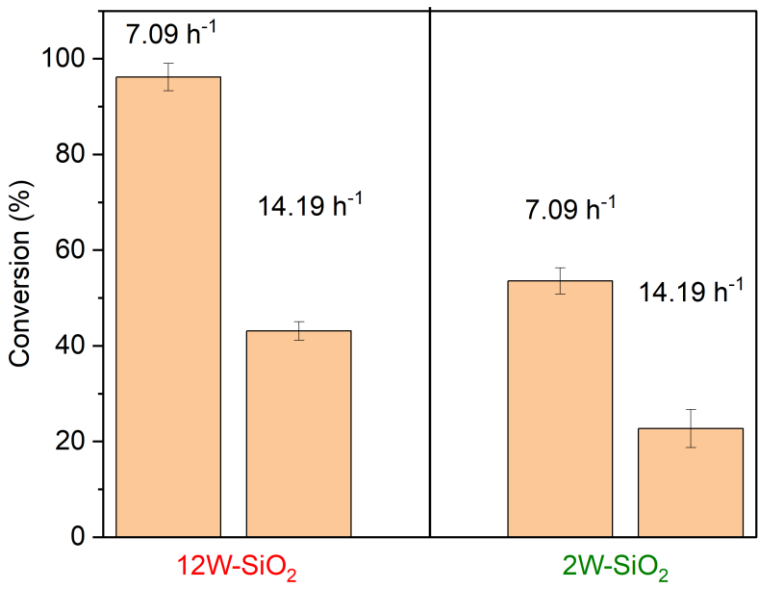

Figure 22S. Average initial ethanol conversion after 5 injections (1 hour) at different WHSV of 7.09 and 14.19 h^{-1}.

To address the concern regarding mass transfer limitations, we estimated theoretical criteria for maintaining kinetic control (i.e., Weisz-Prater and Mears criteria). The threshold criteria were evaluated based on the maximum ethanol conversion rates (i.e., the initial conversion rates at 420 °C). Refer to Table 5S for a summary of the values used to estimate mass transfer criteria.

Table 5S. Summary of the values for computing mass transfer criteria.

Physical quantity	Symbol	Value	Notes
Catalyst particle radius (2W-SiO_2)	r_p	3.3×10^{-7} m	Figure 8S
Catalyst particle radius (6W-SiO_2)	r_p	2.0×10^{-7} m	Figure 8S
Catalyst particle radius (12W-SiO_2)	r_p	1.4×10^{-7} m	Figure 8S
Average pore diameter for catalyst	d_p	1.1×10^{-9} m	
Bulk ethanol concentration	C_A	$4.6\ \mathrm{mol/m^3}$	From ideal gas law
Reynolds number	Re	11	
Schmidt number	Sc	0.34	
Bulk gas diffusivity	D_b	$1.0 \times 10^{-4}\ \mathrm{m^2/s}$	Typical value for ideal gas mixtures
Mass transfer coefficient (2W-SiO_2)	k_m	9.1×10^{2} m/s	$Sh = k_m(2r_p)/D_{AB} = 2 + Re^{1/2} \cdot Sc^{1/3}$ for laminar flow over a sphere
Mass transfer coefficient (6W-SiO_2)	k_m	1.5×10^{3} m/s	$Sh = k_m(2r_p)/D_{AB} = 2 + Re^{1/2} \cdot Sc^{1/3}$ for laminar flow over a sphere
Mass transfer coefficient (12W-SiO_2)	k_m	2.2×10^{3} m/s	$Sh = k_m(2r_p)/D_{AB} = 2 + Re^{1/2} \cdot Sc^{1/3}$ for laminar flow over a sphere
Knudsen diffusivity	D_K	$4.1 \times 10^{-7}\ \mathrm{m^2/s}$	$\bar{\upsilon} d_p/3$
Effective diffusivity	D_e	$4.1 \times 10^{-7}\ \mathrm{m^2/s}$	$D_e = 1/(1/D_b + 1/D_K)$
Density of catalyst support	ρ_s	$1.6 \times 10^{3}\ \mathrm{kg/m^3}$	Approximated as density of crystalline silica multiplied by porosity of 0.4
Observed reaction rate (volumetric) (2W-SiO_2)	r'''	$33\ \mathrm{mol/m^3_{cat} \cdot s}$	From $r = 2.1\times10^{-5}$ mol/g_{cat}·s
Observed reaction rate (volumetric) (6W-SiO_2)	r'''	$42\ \mathrm{mol/m^3_{cat} \cdot s}$	From $r = 2.7\times10^{-5}$ mol/g_{cat}·s
Observed reaction rate (volumetric) (12W-SiO_2)	r'''	$59\ \mathrm{mol/m^3_{cat} \cdot s}$	From $r = 3.7\times10^{-5}$ mol/g_{cat}·s

The threshold criteria were computed via Eq. S1 and S2. Eq. S1 was taken from *Kinetics of Catalytic Reactions* by Vannice,[6] and equation S2 were taken from *The Microkinetics of Heterogeneous Catalysis* by Dumesic.[7] All the estimated criteria are significantly below the limitation criteria (Table 6S), indicating the reported rates (< 3.7×10^{-5} mol/g_{cat}·s) are free of mass transfer limitations.

Weisz-Prater Criteria for excluding intraparticle mass transfer limitations:

$$\frac{R''' \times {r_P}^2}{C_A \times D_e} = Weisz - Prater\ criterion\ (should\ be\ < 0.3) \qquad \text{(Eq. S1)}$$

Criteria for excluding interphase mass transfer limitations:

$$\frac{r''' r_P}{C_A k_m} = Mears\ criterion\ (should\ be\ < 0.15) \qquad \text{(Eq. S2)}$$

Table 6S. Summary of the values of mass transfer criteria

Sample	Weisz-Prater criterion	Mears criterion
2W-SiO_2	1.9×10^{-6}	2.6×10^{-9}
6W-SiO_2	8.9×10^{-7}	1.2×10^{-9}
12W-SiO_2	6.1×10^{-7}	8.3×10^{-10}

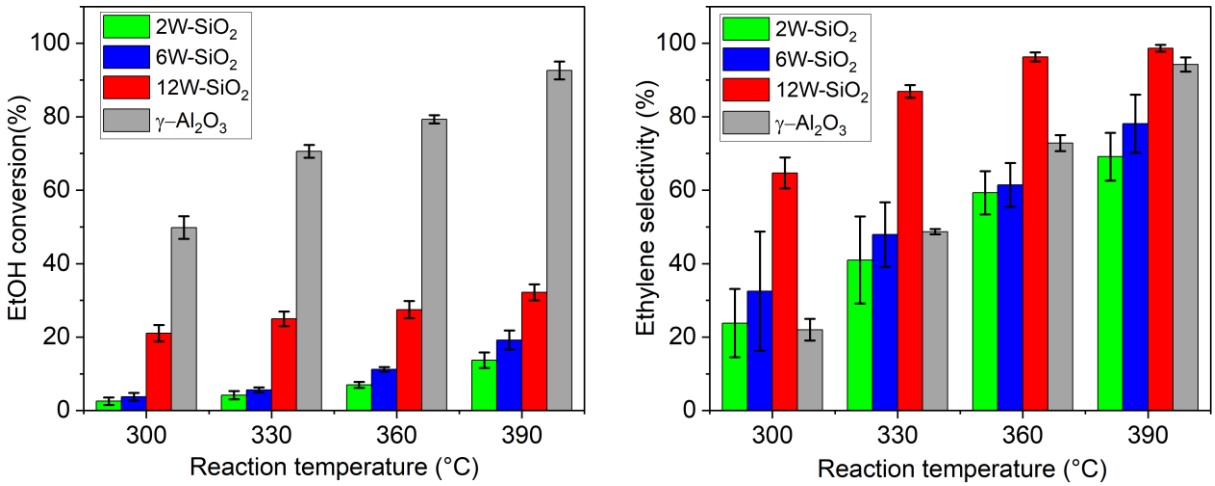

Figure 23S. Average values of ethanol conversion (left) and ethylene selectivity (right) at temperatures 300-390 °C. Data are obtained from 5 measurements at each temperature with error bars.

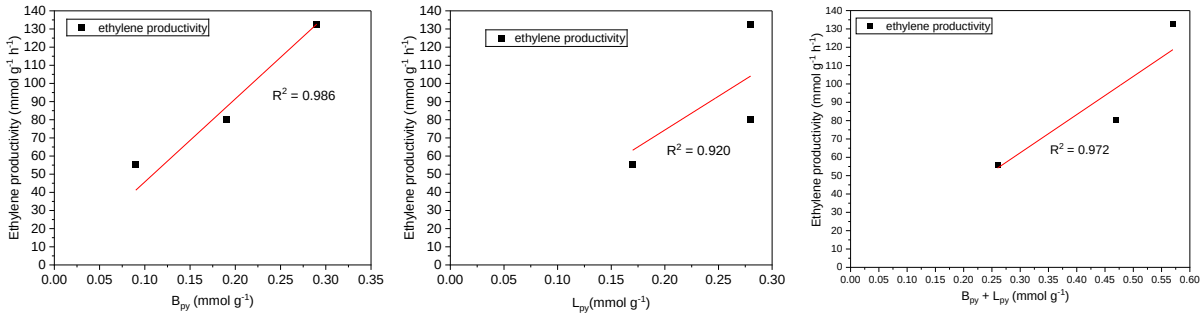

Figure 24S. Correlation of initial ethylene productivity at 420 °C with number of Brönsted (B_{py}), Lewis (L_{py}), and total (B_{py} + L_{py}) acid sites.

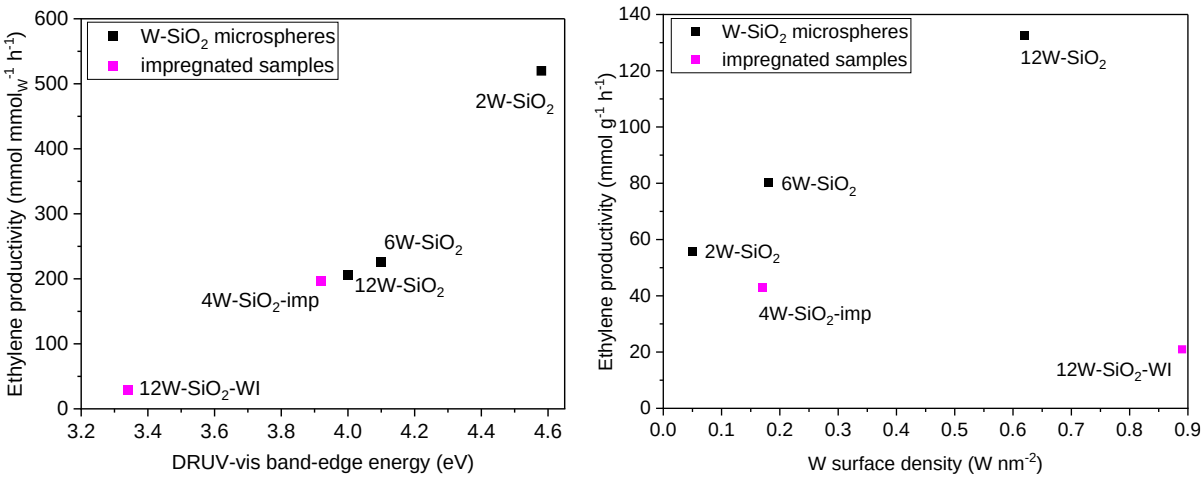

Figure 25S. Correlation of initial ethylene productivity with DRUV-Vis band-edge energy (left) and tungsten surface density from XPS (right).

3.1 Tungsten molar content normalized ethylene production

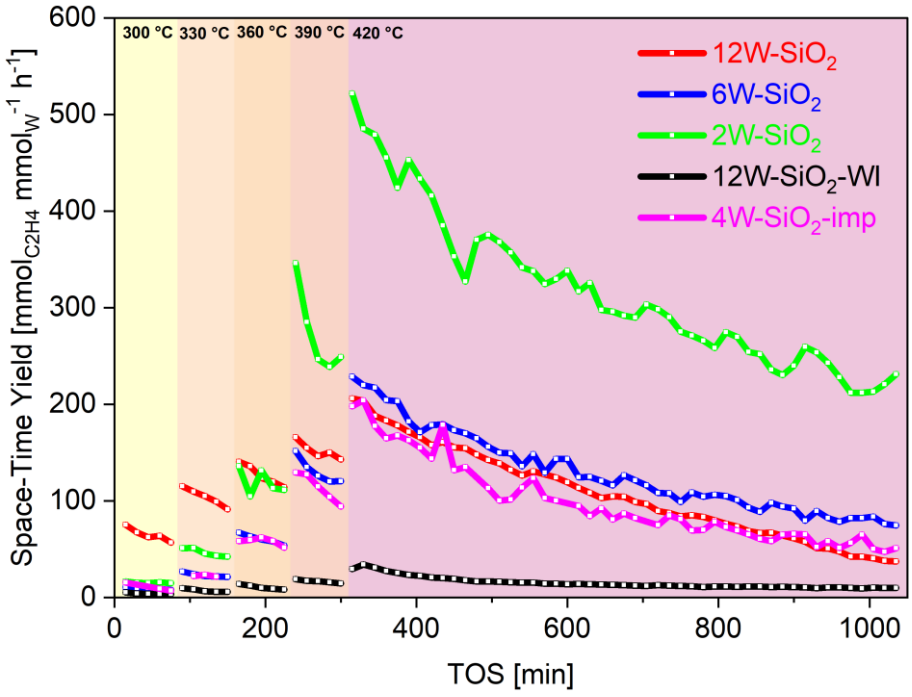

Figure 26S. The activity of the catalysts related to the molar content of tungsten. Expressed as space-time yield.

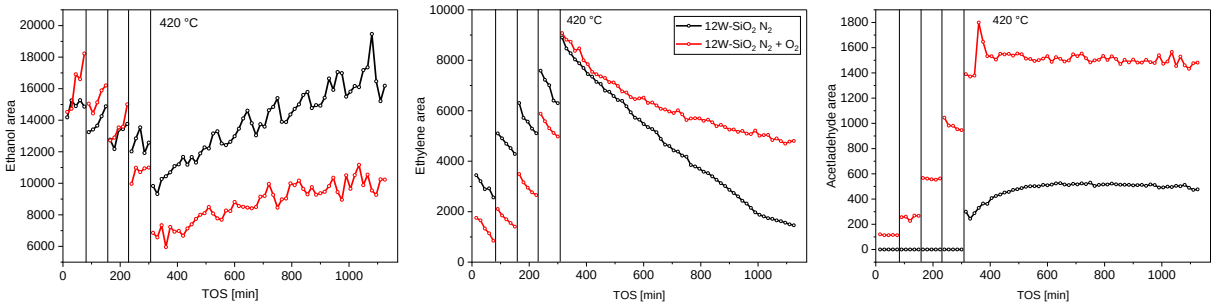

Figure 27S. Ethanol, ethylene, and acetaldehyde peak areas during the ethanol dehydration performed under nitrogen and mixed nitrogen/oxygen atmosphere.

Partial over-oxidation of pentane and ethanol to CO, CO_2, and other products cannot be avoided under the reaction conditions strongly affecting carbon balance. Therefore, ethanol conversion and product selectivities and yields were not calculated and only peak areas are given for the sake of comparison.

3.2 Spent catalysts

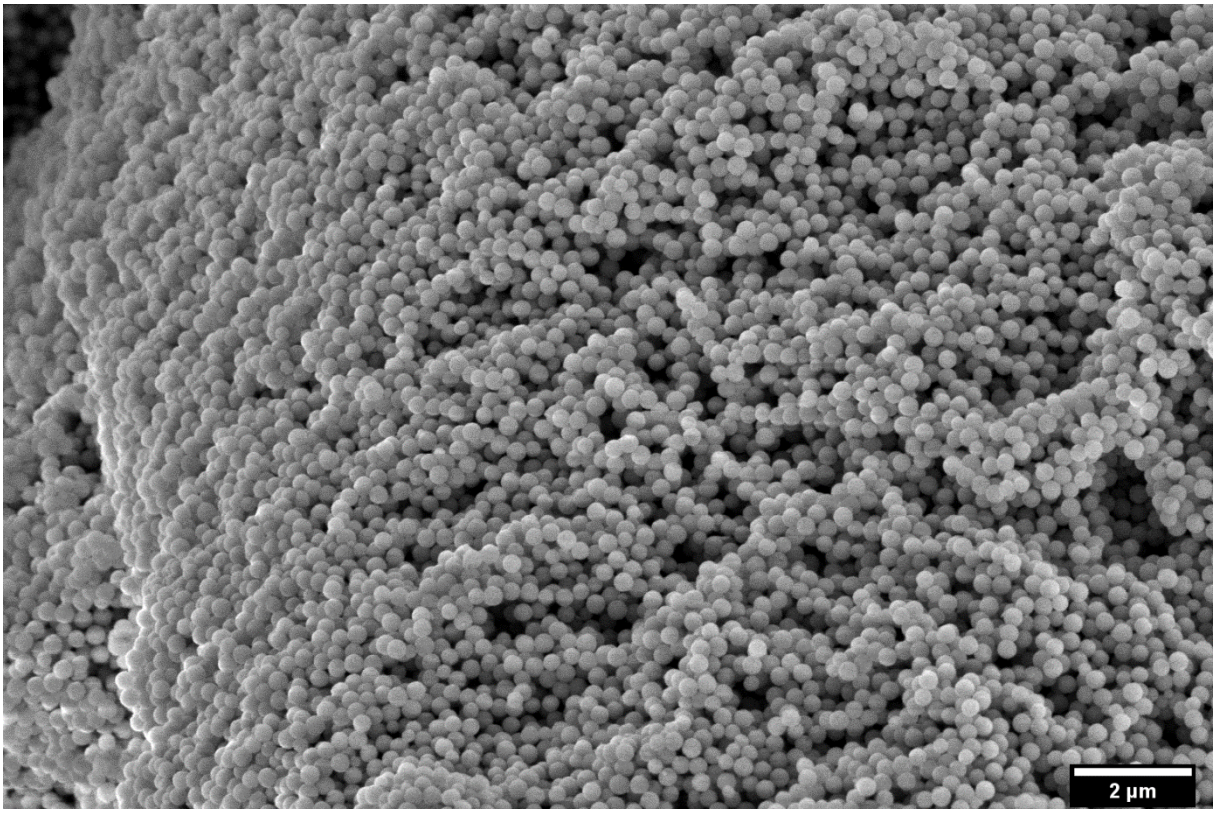

Figure 28S. SEM image of 12W-SiO_2 spent catalyst.

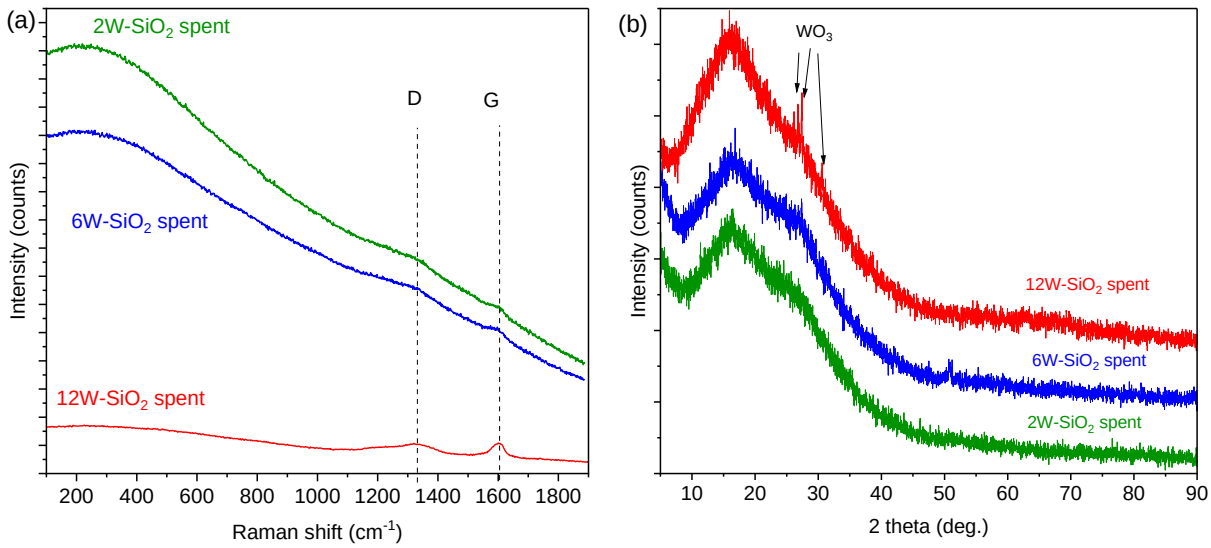

Figure 29S. Raman spectra (a) and PXRD diffractograms (b) of 12W-SiO₂, 6W-SiO₂, and 2W-SiO₂ spent catalysts.

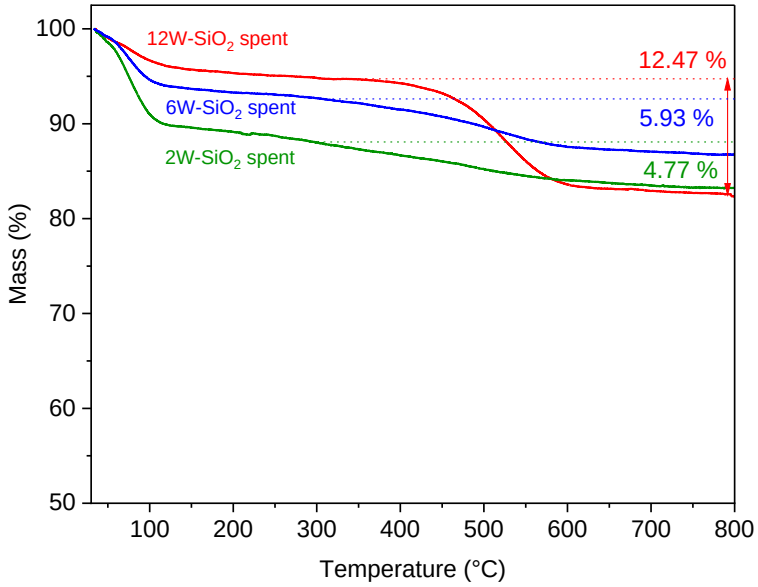

Figure 30S. TG curve of 12W-SiO₂ spent catalyst (performed in the atmosphere of air).

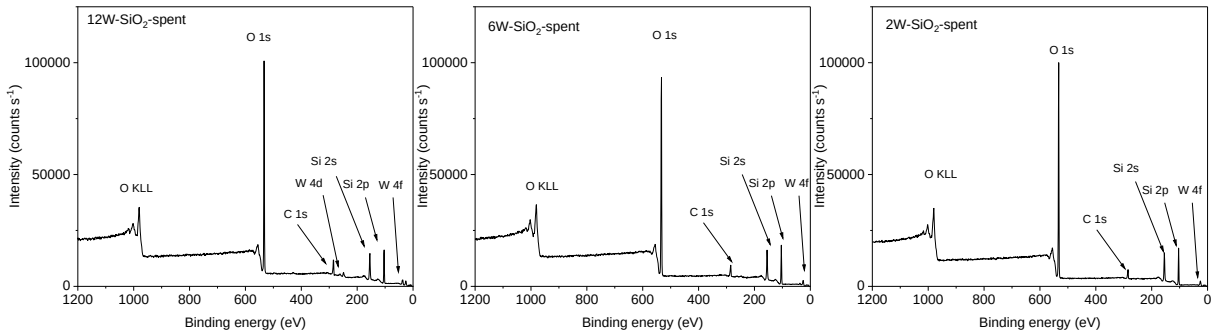

Figure 31S. Wide XPS scans of spent W-SiO₂ catalysts.

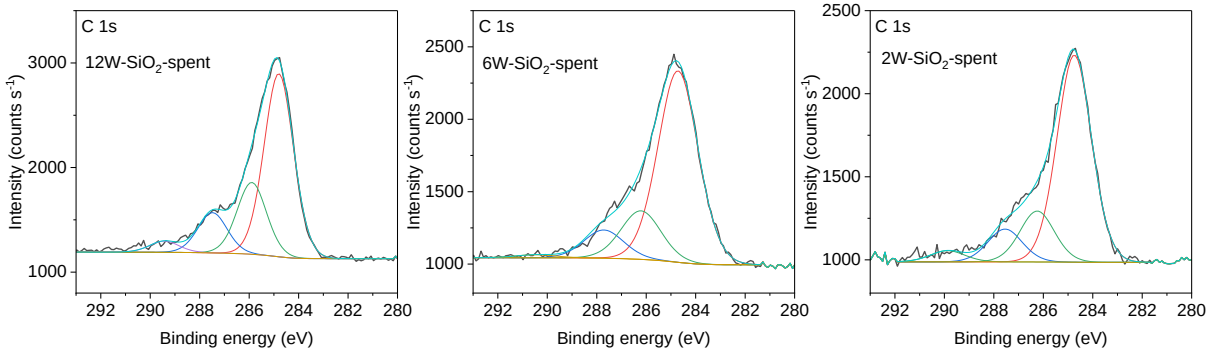

Figure 32S. C 1s XPS spectra of spent W-SiO₂ catalysts.

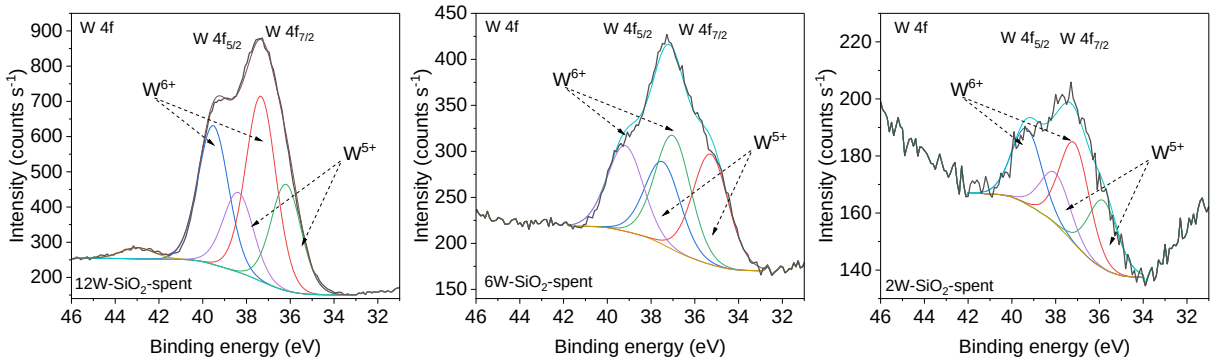

Figure 33S. W 4f XPS spectra of spent W-SiO₂ catalysts.

Table 7S. Surface composition of fresh and spent catalysts determined by XPS.

	wt.% XPS			
sample	W	Si	O	C
2W-SiO_2-spent	0.45	55.6	35.56	4.89
6W-SiO_2-spent	2.44	55.6	35.56	6.40
12W-SiO_2-spent	7.72	50.54	33.92	7.82

Table 8S. Ratio of W^{6+}/W^{5} 4f peak areas from XPS spectra of fresh and spent W-SiO₂ catalysts.

catalyst	W^{6+}/W^{5+}	
	fresh	spent
12W-SiO_2	3.48	1.75
6W-SiO_2	2.57	1.03
2W-SiO_2	2.63	1.48

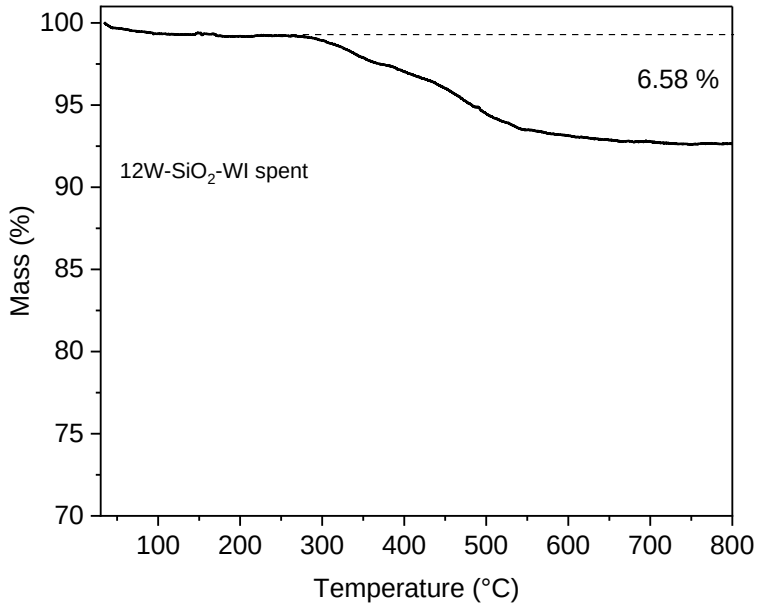

Figure 34S. TGA analysis of 12W-SiO_2-WI spent reference catalyst prepared via impregnation technique.

References

1 Dhumal, N. R.; Singh, M. P.; Anderson, J. A.; Kiefer, J.; Kim, H. J. Molecular Interactions of a Cu-Based Metal–Organic Framework with a Confined Imidazolium-Based Ionic Liquid: A Combined Density Functional Theory and Experimental Vibrational Spectroscopy Study. *J. Phys. Chem. C* 2016, **120** (6), 3295–3304. https://doi.org/10.1021/acs.jpcc.5b10123.

2 Liu, B.; Zou, R.-Q.; Zhong, R.-Q.; Han, S.; Shioyama, H.; Yamada, T.; Maruta, G.; Takeda, S.; Xu, Q. Microporous Coordination Polymers of Cobalt(II) and Manganese(II) 2,6-Naphthalenedicarboxylate: Preparations, Structures and Gas Sorptive and Magnetic Properties. *Microporous Mesoporous Mater.* 2008, **111** (1–3), 470–477. https://doi.org/10.1016/j.micromeso.2007.08.024.

3 Huang, Y.; Jiang, Z.; Schwieger, W. Vibrational Spectroscopic Studies of Layered Silicates. *Chem. Mater.* 1999, **11** (5), 1210–1217. https://doi.org/10.1021/cm980403m.

4 Zaki, M. I.; Mekhemer, G. A. H.; Fouad, N. E.; Rabee, A. I. M. Structure–Acidity Correlation of Supported Tungsten(VI)-Oxo-Species: FT-IR and TPD Studies of Adsorbed Pyridine and Catalytic Decomposition of 2-Propanol. *Appl. Surf. Sci.* 2014, **308**, 380–387. https://doi.org/10.1016/j.apsusc.2014.04.180.

5 Skoda, D.; Hanulikova, B.; Styskalik, A.; Vykoukal, V.; Machac, P.; Urbanek, P.; Domincova Bergerova, E.; Simonikova, L.; Kuritka, I. Non-Aqueous Synthesis of Homogeneous Molybdenum Silicate Microspheres and Their Application as Heterogeneous Catalysts in Olefin Epoxidation and Selective Aniline Oxidation. *J. Ind. Eng. Chem.* 2022, **107**, 320–332. https://doi.org/10.1016/j.jiec.2021.12.001.

6 Vannice, M. A.; Joyce, W. H. *Kinetics of Catalytic Reactions*; Springer US: Boston, MA, 2005. https://doi.org/10.1007/b136380.

7 Dumesic, J. A.; Rudd, D. F.; Aparicio, L. M.; Rekoske, J. E.; Trevino, A. A. *The Microkinetics of Heterogeneous Catalysis*, 1st Editio.; American Chemical Society, 1993.